Measurement of Kinetic-Scale Current Filamentation Dynamics and Associated Magnetic Fields in Interpenetrating Plasmas

G. F. Swadling,[1,*] C. Bruulsema,[2,3] F. Fiuza,[3] D. P. Higginson,[1] C. M. Huntington,[1] H-S. Park,[1] B. B. Pollock,[1] W. Rozmus,[3,2] H. G. Rinderknecht,[4] J. Katz,[4] A. Birkel,[5] and J. S. Ross[1]

[1]*Lawrence Livermore National Laboratory, Livermore, California 94551, USA*
[2]*Department of Physics, University of Alberta, Edmonton, Alberta, Canada T6G 2E1*
[3]*SLAC National Accelerator Laboratory, Menlo Park, California 94025, USA*
[4]*Laboratory for Laser Energetics, University of Rochester, Rochester, New York 14623, USA*
[5]*Plasma Science and Fusion Center, Massachusetts Institute of Technology, Cambridge, Massachusetts 02139, USA*

(Received 16 April 2019; revised manuscript received 20 September 2019; accepted 5 May 2020; published 27 May 2020)

We present the first local, quantitative measurements of ion current filamentation and magnetic field amplification in interpenetrating plasmas, characterizing the dynamics of the ion Weibel instability. The interaction of a pair of laser-generated, counterpropagating, collisionless, supersonic plasma flows is probed using optical Thomson scattering (TS). Analysis of the TS ion-feature revealed anticorrelated modulations in the density of the two ion streams at the spatial scale of the ion skin depth $c/\omega_{pi} = 120\ \mu$m, and a correlated modulation in the plasma current. The inferred current profile implies a magnetic field amplitude $\sim 30 \pm 6$ T, corresponding to $\sim 1\%$ of the flow kinetic energy, indicating that magnetic trapping is the dominant saturation mechanism.

DOI: 10.1103/PhysRevLett.124.215001

Magnetic field amplification and shock formation by streaming plasma instabilities associated with supersonic plasma flows are ubiquitous in astrophysical environments. For low-density astrophysical plasmas, the ion-ion collisional mean free path ($\ell_s^{i\backslash i}$) can often be much larger than the size of the systems of interest. This implies that the processes that dominate the plasma dynamics must be "collisionless," i.e., that deceleration of plasma flows and scattering of particles must be mediated by electric (E) or magnetic (B) fields generated through plasma instabilities driven by the interpenetration of counterpropagating flows. The scales at which these microphysical plasma instabilities operate cannot be resolved by astronomical observation. Over the last decade this has motivated a significant effort to develop high energy density (HED) laboratory astrophysics experiments that can probe these fundamental plasma processes in a controlled environment and benchmark theoretical and numerical models [1–24].

The ion-Weibel or current filamentation instability is believed to be the dominant mechanism for B-field generation, amplification, and shock formation in weakly magnetized environments such as young supernova remnant shocks and gamma-ray bursts [25–27,3]. It is a fundamental plasma instability driven by an anisotropy in the ion velocity distribution, analogous to the electron instability described by Weibel [28] and Fried [29]. Growth of this instability is believed to drive filamentation of interpenetrating ion streams, with wave vectors perpendicular to the flow velocities and with the most unstable wavelengths at around the ion skin depth scale (c/ω_{pi}); its growth amplifies plasma currents and corresponding B fields. Despite the recognized importance of this instability and very active theoretical and numerical research over the past two decades, its experimental characterization has proven challenging. Previous experiments based on proton radiography [10,17] could only provide path integrated measurements affected by both B and E fields and relied on plasma simulations to interpret the corresponding field structure. Until now, direct, local experimental characterization of the plasma currents and associated B fields at the kinetic scale has remained elusive.

In this Letter we present data from novel experiments in which optical Thomson scattering (TS) is used to make the first direct, quantitative measurements of transverse modulations in the plasma current density $\vec{J}$ at the scale of the ion skin depth c/ω_{pi}. This $\vec{J}$ is used to infer the strength of B fields in the plasmas. We show that by fitting the profiles of the measured TS spectra it is possible to infer both the velocities and relative densities of the two ion streams and the resultant $\vec{J}$ associated with the ion Weibel instability. The observed $\vec{J}$ modulation reveals a near complete separation of the opposing flows at the ion skin depth scale. This corresponds to an average magnetic energy density of $\sim 1\%$ of the flow kinetic energy density, indicating magnetic trapping as the dominant saturation mechanism [30]. These findings have important implications for understanding the strength of the magnetic fields produced in astrophysical plasma and provide critical data for benchmarking numerical and theoretical models.

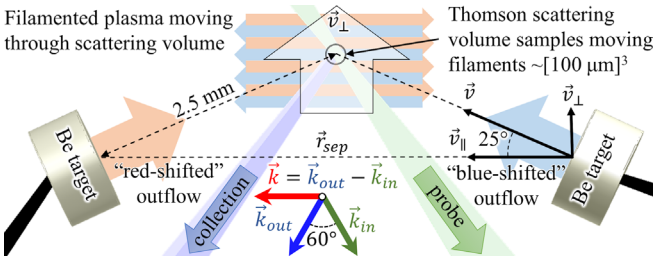

FIG. 1. Experimental setup. Green and blue arrows indicate OTS probe and collection vectors, respectively. Red arrow shows corresponding scattering wave vector.

Experiments were conducted at the 60 beam OMEGA laser facility at the Laboratory for Laser Energetics, University of Rochester. Figure 1 shows a schematic of the setup. A pair of 1 mm diameter, 500 μm thick beryllium disks are simultaneously heated by ~3.5 kJ, 1 ns square shaped laser pulses (7 beams per target, 351 nm wavelength, 300 μm diameter spot, $\sim 5 \times 10^{15}$ W cm^{-2} intensity). These parameters are similar to those used in previous experiments investigating Weibel growth in interpenetrating plasmas [7,9,12,17,19]. Plasma expands from the surface of each target with a peak velocity of ~1500 km s^{-1}. The novel aspect of these experiments is that the surface normals of the two target disks are tilted 25° from the vector linking the target centers ($\vec{r}_{\rm sep}$). The outflow velocity $\vec{v}$ of each flow may therefore be decomposed into components parallel ($\vec{v}_{\parallel}$) and perpendicular ($\vec{v}_{\perp}$) to $\vec{r}_{\rm sep}$.

The TS diagnostic collects scattered light from a volume located at the intersection of the two target-center-normal vectors. The size of the TS volume is defined by the spectrometer input pinhole (~100 μm) and the diameter of the probe beam focus (~70 μm). A $\lambda_0 = 526.5$ nm probe beam ($\vec{k}_{\rm in}$, ~50 J, 1 ns, $f/6.7$) points through this volume at 60° from $\vec{v}_{\parallel}$ and scattered light is collected ($\vec{k}_{\rm out}(\lambda)$, $f/10$) at a scattering angle of $\theta = 60°$, such that the wave vectors of the probed density fluctuations ($\vec{k} = \vec{k}_{\rm out} - \vec{k}_{\rm in}$) lie parallel to and are sensitive to the $\vec{v}_{\parallel}$ of each flow. Doppler shifts induced by the flow velocities of the two ion populations ($\vec{v}_j$) are therefore of opposite sign ($\delta\omega = \vec{k} \cdot \vec{v}_j$), so that spectral features associated with scattering from each flow are separated spectrally and can be observed independently. The tilted geometry means that the plasma stream interaction takes place in an inertial frame moving transversely at velocity $\vec{v}_{\perp}$ with respect to the static TS measurement volume. Any filamentary plasma structure that develops through the growth of the Weibel instability is therefore scanned through the TS scattering volume at $\vec{v}_{\perp}$, as indicated in Fig. 1.

Collected light is dispersed using a pair of Czerny-Turner imaging spectrometers, configured to measure the narrowband ($\Delta\lambda \sim 6$ nm) ion acoustic wave (IAW) and the broadband ($\Delta\lambda \sim 300$ nm) electron plasma wave (EPW) features of the TS spectrum [31,32]. ROSS optical streak cameras record the scattered spectra, providing ~100 ps temporal resolution over the duration of the TS probe laser pulse.

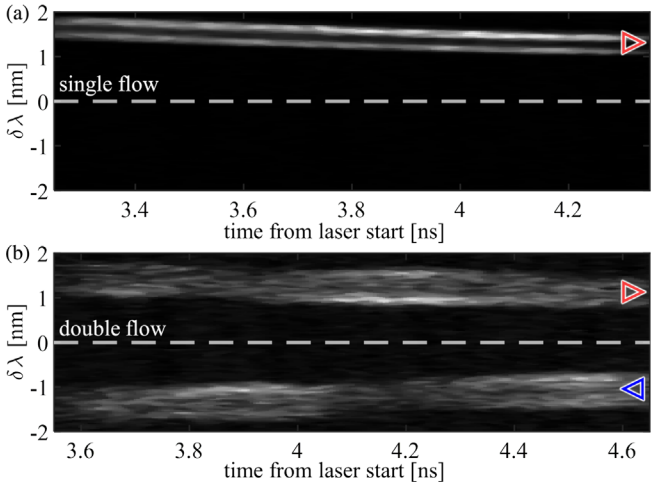

FIG. 2. Streaked IAW spectra for (a) single- and (b) double-flow experiments, plotted against wavelength shift $\delta\lambda = \lambda - \lambda_0$. Red and blue triangles indicate redshifted and blueshifted spectral features.

A series of experiments were carried out to investigate the flow interactions. Figure 2 shows examples of IAW spectrograms recorded in both a single flow (a) and a double flow (b) experiment which are characteristic of our experimental results (see Ref. [33] for further examples). In single flow experiments only one of the targets is laser heated, allowing characterization of an individual plasma flow. In the single flow spectrogram, the narrow, double-peaked, redshifted spectral feature corresponds to scattering from the single ion stream. The double-peaked structure is characteristic of IAW spectral features, corresponding to collective scattering on IAWs propagating both parallel and antiparallel to $\vec{k}$ [32]. The overall doppler shift of the IAW feature is proportional to $\vec{v}_{\parallel}$. For the scattering geometry used in this experiment $|\delta\lambda| \approx \lambda_0 |\vec{v}_{\parallel}|/c$, and therefore the observed $|\delta\lambda| \sim 1.5 \pm 0.2$ nm spectral shift corresponds to $\vec{v}_{\parallel} \approx 850 \pm 110$ km s^{-1}. Geometrically we can infer $|\vec{v}| \approx 940 \pm 130$ and $\vec{v}_{\perp} \approx 400 \pm 50$ km s^{-1}.

The double flow spectrogram [Fig. 2(b)] contains an additional blueshifted, double-peaked spectral feature, corresponding to scattering from the additional, counter-propagating ion stream. The spectral separation of the two ion features indicates that the ion streams are interpenetrating as expected. The magnitude of the $\delta\lambda$ as a function of time for each of the two peaks is approximately equal to that measured in the single flow experiment, indicating the flows have not been significantly slowed due to their interaction. The increased separation of the sub-peaks of each IAW feature indicates the electron temperature (T_e) is higher in the double flow experiment, as seen in previous experiments [12]. Electrons are heated through friction with

the interpenetrating ion streams and that heat is transferred to the ions via anomalous wave-particle interactions, with fluctuations enhanced by the ion two-stream instability [12] and later the ion Weibel instability [30,34,35], driving broadening of the peaks.

The novel feature observed in this experiment is the anticorrelated temporal modulation in the intensity of the spectral features corresponding to the two interpenetrating flows seen in Fig. 2(b). In the absence of transverse flow modulations, the TS IAW feature for a pair of symmetric, interpenetrating flows should be symmetric about λ_0. The brightness of the two ion-acoustic features are modulated and these modulations are anticorrelated in time. This modulation in the IAW features was observed in all of a series of four tilted geometry double flow experiments [33]. The intensity of each IAW feature is a strong function of the ion density n_j of the corresponding stream; therefore the observed modulation is consistent with modulations in the ion density of the two streams that would be expected due to the growth of the ion-Weibel filamentation instability. The period for a single modulation in the IAW intensity is $\sim 0.6 \pm 0.05$ ns, assessed from the IAW data from all four shots [33]. The plasma moves through the TS volume at $\vec{v}_\perp$ (estimated above), so the inferred scale length of the modulations in the plasma causing this modulation is $\sim 240 \pm 40$ μm in direction $\hat{v}_\perp$. In contrast, no oscillation was observed in any of three single flow experiments, indicating that the modulation in the double flow data must be induced by the interaction of the two flows.

Fits to simultaneously measured EPW spectra provide measurements of the electron density, $n_e \sim 1.7 \pm 0.2 \times 10^{19}\,\mathrm{cm}^{-3}$ (total, double flow) and temperature $T_e \sim 600 \pm 50$ eV [33]. The average ion density of a single stream can be estimated $n_i = n_e/(2\bar{Z})$, where $\bar{Z}$ is the average ionization state, so that the ion plasma frequency is $\omega_{pi} = 2.5 \pm 0.2$ THz and the ion skin depth is $c/\omega_{pi} = 120 \pm 10$ μm. The observed 240 μm modulation wavelength therefore corresponds to a distance $\sim 2(c/\omega_{pi})$. For the ions, intrastream collisions are frequent ($\nu_{ii}^{\mathrm{intra}} \approx 70\ \mathrm{ns}^{-1}$) but interstream collisions are rare ($\nu_{ii}^{\mathrm{inter}} \approx 0.05\ \mathrm{ns}^{-1}$). The ions are therefore treated as two separate Maxwellian populations with mean velocities $\pm\vec{v}_\parallel$. The electron thermal velocity v_{Te} is much larger than the approach velocity of the two streams $2v_\parallel$ and the electron-electron collision frequency is high, therefore the electrons are treated as a single Maxwellian population with mean velocity equal to the mean ion velocity minus the drift velocity corresponding to the plasma current $J = -n_e e v_{\mathrm{Drift}}$. TS spectral data [e.g., Fig. 3(a)] are modeled using the well-known, analytic, nonrelativistic Maxwellian formulation for the structure factor, $S(\vec{k},\omega)$ [32,36],

$$S(\vec{k},\omega) = \frac{2\pi}{|\vec{k}|}\left|1 - \frac{\chi_e}{\epsilon}\right|^2 f_{eo} + \frac{2\pi}{|\vec{k}|}\sum_j \frac{\bar{Z}_j n_j}{n_e}\left|\frac{\chi_e}{\epsilon}\right|^2 f_{jo},$$

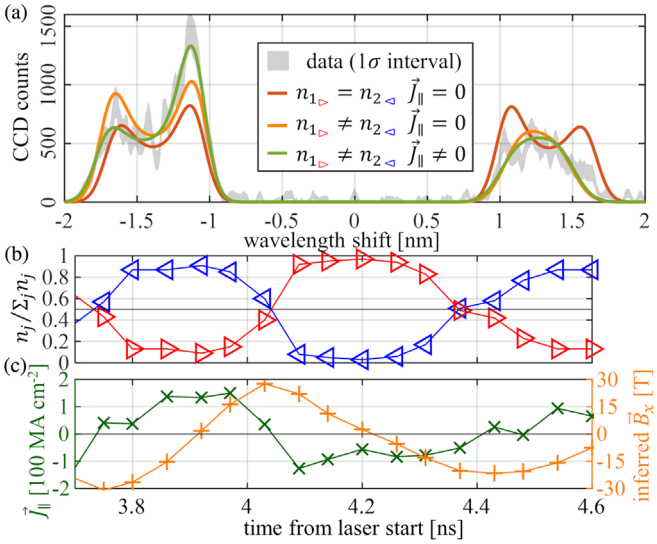

FIG. 3. (a) Examples of TS fits [spectral profile from Fig. 2(b) at $t = 3.8$ ns], showing the effect of allowing different parameters to vary. Fitting a series of profiles taken at regular time intervals reveals modulations in the relative ion stream density $n_j/\sum_j n_j$ (b) and drift current $\vec{J}_\parallel$ (c). The magnetic field profile B_x is inferred from the $\vec{J}_\parallel$ profile. Uncertainty in the determination of the relative ion density was ~10%, and ~20% in the determination of the current. The methods used to determine the uncertainty are discussed in Ref. [33].

where $\epsilon = 1 + \chi_e + \sum_j \chi_j$ is the longitudinal dielectric function, f_{j0}, f_{e0}, χ_j, χ_e are the distribution functions and susceptibilities of the ion populations ($j = 1, 2$) and electrons, respectively, and n_j and $\bar{Z}_j$ are the corresponding densities and ionization states of the ions. Plasma parameters such as n_j are specified locally and therefore can be different, $n_1 \neq n_2$, depending on whether the left or right streaming filament dominates the TS volume. The model assumes that the plasma distribution functions are Maxwellian; this a reasonable approximation given the rapid intra-population Coulomb collision rates, which will act to maintain the distributions' Maxwellian shape [37]. Moreover, a series of OSIRIS [38,39] two dimensional particle-in-cell (PIC) simulations has confirmed that even in the collisionless limit the growth of the ion Weibel instability does not introduce distortions to the distribution functions large enough to have any measurable effect on the TS spectrum [40].

Inspection of $S(\vec{k},\omega)$ indicates the modulation of the two ion peaks observed in Fig. 2(b) is consistent only with a modulation in the relative densities of the two ion populations within the TS volume ($\bar{Z}_j n_j/n_e$ term). These modulations in the relative density correspond to ion current density modulations $\vec{J}_i = \sum_j v_{\parallel j} n_j \bar{Z}_j e$ in the direction transverse to the relative velocity of the two interpenetrating plasma flows ($\hat{v}_\perp$). These modulations are therefore consistent with filamentation driven by the

ion-Weibel instability, as observed in numerous simulations and theoretical studies [3,17,34,35]. The observed scale length of 240 μm agrees reasonably well with estimates from proton radiography [22] and is also in reasonable agreement with theory [8,30,41], which predicts a peak growth rate $\Gamma \sim 5.5$ ns^{-1} at $v_{\parallel} = 800$ km s^{-1}, and wave vector $k_y \sim 5 \times 10^4$ m^{-1}, corresponding to a scale size $2\pi/k_y \sim 120$ μm. The interpretation that the modulation is due to filamentation is further corroborated by data from >10 experiments where the targets were oriented directly facing [33].

The Thomson data was fitted using $S(\vec{k}, \omega)$. The plasma was modeled using two fully ionized, counterpropagating, $^9_4$Be ion populations and a single electron population with $n_e = 1.55$–1.90×10^{19} cm^{-3}. Separate $|\vec{v}_{\parallel j}|$ values were defined for the two flows, and the T_i were defined equal based on symmetry arguments. Fitting parameters T_e, T_i, $\bar{Z}_j n_j/n_e$, $|\vec{v}_{\parallel j}|$, and $\vec{J}_{\parallel} = \hat{k} \cdot \vec{J}$ were varied to optimize the fit to the data using a Newton-Gauss nonlinear regression algorithm [33]. Figure 3(a) shows fits to a spectral profile from Fig. 2(b) taken at 3.8 ns (binned over 0.1 ns), illustrating how the relative amplitude of the two ion features provides diagnostic access to the $n_j/\sum_j n_j$ of the left- and right-flowing streams (red → orange fit), while the relative widths and amplitudes of the IAW subpeaks within each redshifted and blueshifted feature provide a diagnostic of the net $\vec{J}_{\parallel}$ (orange → green fit). The variations in the plasma parameters resulting from fitting a series of such profiles over time are presented in Figs. 3(b) and 3(c). The uncertainty in our fits is dominated by the low signal to noise of the measured signal. The trends in $n_j/\sum_j n_j$ with time for the two flows [Fig. 3(b)] shows an approximately sinusoidal modulation. The fitting revealed that this modulation in $n_j/\sum_j n_j$ is spatially correlated to a modulation in $\vec{J}_{\parallel}$ [Fig. 3(c)]. The peak ion current in the center of a "filament" is $|\vec{J}_i| = 190 \pm 20$ MA cm^{-2}. The peak plasma current amplitude at the center of a filament is $|\vec{J}_{\parallel}| = 160 \pm 30$ MA cm^{-2}, comparable to the ion current, indicating that current screening by the electron population is small. It should be noted that the TS measurements are spatially integrated over the ~100 μm scale size of the TS volume, and therefore the inferred filamentation contrast should be treated as a lower limit.

The time-averaged value of the magnitude of the current density modulation is $\sim 90 \pm 20$ MA cm^{-2}. Based on the above estimated ~100 μm scale size of the filaments (50 μm radius), we estimate each filament carries $I \sim \pi r^2 |\vec{J}_{\parallel}| = 7.3 \pm 1.5$ kA, and is surrounded by an azimuthal magnetic field whose strength is $B \sim \mu_0 I/2\pi r = 30 \pm 6$ T. This allows us to place constraints on the saturation mechanism associated with the ion Weibel instability. Different mechanisms have been discussed in the literature, with the most common being the Alfvén limit [42], where the ion gyroradius equals the filament wavelength, $B_A \sim m_i v_i/Ze\lambda_y$, and magnetic trapping [30], where the bouncing frequency of the ions inside the filaments equals the growth rate of the Weibel instability, $B_T \sim (m_i v_i/Ze)(\omega_{pi}/c)^2(\lambda_y/2\pi)$. For the parameters of our experiments, $B_A \sim 90$ and $B_T \sim 50$ T. Thus, our results favor magnetic trapping as the dominant saturation mechanism for the ion Weibel instability.

The mean B-field energy density in the plasma is $\sim |B^2|/2\mu_0 = 0.18 \pm 0.06$ kJ cm^{-3}. For comparison, the average kinetic energy density of each of the incoming flows is $n_e m_i v_i^2/4\bar{Z} \sim 15$ kJ cm^{-3}, ion thermal energy is $3n_e k_B T_i/(2\bar{Z}) \sim 0.32$ kJ cm^{-3}, and electron thermal energy is $3n_e k_B T_e/2 \sim 2.5$ kJ cm^{-3}. The entrained magnetic field energy therefore represents ~1% of the system energy, consistent with the saturation level found in some of the previous simulation studies [3,17]. Given that the filaments drift through the TS volume at velocity $\vec{v}_{\perp} = \hat{y} v_{\perp}$ and carry current with uniform current density $\vec{J}_{\parallel} = \hat{z} J_{\parallel}$, the B_x component of the azimuthal magnetic field should satisfy the approximate equation, $\partial B_x/\partial y = \mu_0 J_{\parallel}/2$. Integrating this equation gives the B_x profile shown in Fig. 3(c). The x component of the magnetic field reaches its maximum value, ~30 T, where the net current is zero, i.e., at the boundary of two opposed ion current filaments.

The experimental results allow us to benchmark large-scale 3D PIC simulations, typically used in the study of the Weibel instability. We have performed simulations that model the interaction of two collisionless plasma flows, each having ion density $n_0/2$ and approach velocities $\pm\vec{v}_0$. The collision geometry was matched to that used in the experiments. The interaction volume was $8 \times 8 \times 8 (c/\omega_{pi})^3$, resolved using 128^3 cells, with 32 particles per cell. A reduced mass-to-charge ratio $m_i/(m_e\bar{Z}) = 128$ and increased flow velocity $v_0 = 0.1$ c were used to accelerate the 3D simulation; this is common practice in numerical studies of the Weibel instability in nonrelativistic flows due to computational constraints. We note that for the conditions of our study, the physics of electromagnetic instabilities is independent of the flow velocity, provided it is nonrelativistic. The evolution of two systems with velocity v_1 and v_2 scales such that these systems should be similar at times $t_2 = t_1 v_1/v_2$ [8]. This scaling is used to compare the simulations with the experimental results at 4.2 ns in Fig. 3. Figure 4 shows section views of the plasma current modulation taken through the simulation data cube at this time, illustrating the 3D nature of the filamentary structures formed in these interpenetrating plasmas. The $\sim 2c/\omega_{pi}$ spatial scale of the ion density (c) and current (d) modulations in the simulated plasma compare very well with the $2c/\omega_{pi}$ observed in the experiment [Figs. 3(c) and 3(d)]. The filamentation contrast and current amplitude are also in good agreement.

Our results provide the first direct local measurements of the counterstreaming currents and associated dynamics at

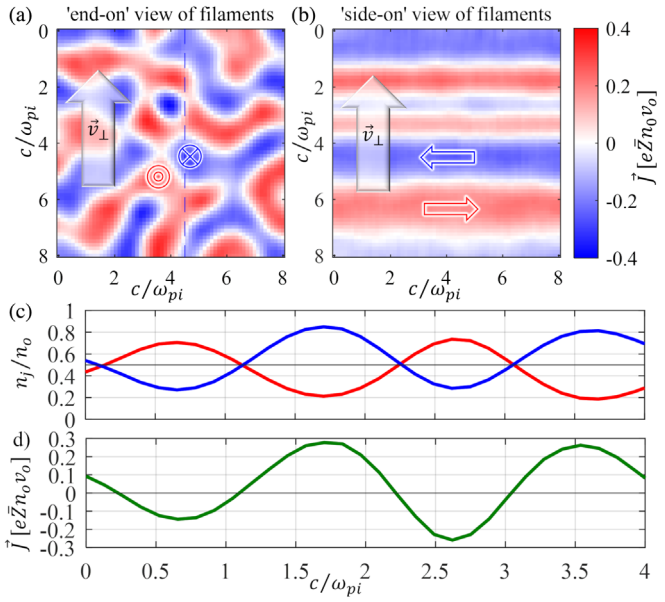

FIG. 4. 3D PIC simulations. (a) "End-on" view of filamented plasma, showing modulation in plasma current. (b) "Side-on" slice [position marked by dashed line in (a)]. The arrows superimposed over these images indicate the flow velocity of the plasma structure in the lab frame induced by the tilted target geometry and the current direction. (c) Spatial profile of the ion density modulation of the two streams and (d) plasma current. In the experiment $c/\omega_{pi}\sim 120\ \mu$m and $e\bar{Z}n_0v_0 \sim 200$ MA cm^{-2}.

the ion skin depth scale length associated with the ion Weibel instability. The collisionless physics underlying the development of electromagnetic instabilities such as the ion Weibel instability can be rigorously scaled with plasma density and flow velocity [8] such that data from these laboratory experiments may be used to test analytical and numerical models of physical phenomena observed at the astrophysical scale. Based on these measurements we were able to infer the magnetic field produced in the plasma and identify magnetic trapping as the dominant saturation mechanism of this fundamental plasma instability. The Thomson scattering based technique employed to infer the current locally in HED plasmas is novel and opens a new way to directly probe the microphysics of electromagnetic plasma instabilities in HED experiments, relevant to a wide range of problems, from laboratory astrophysics to laser-plasma accelerators [43] to inertial confinement fusion [44]. In future work, we plan to use this technique to make direct measurements of the growth rate and nonlinear evolution of the ion Weibel instability.

This work was performed under the auspices of the U.S. Department of Energy by Lawrence Livermore National Laboratory (LLNL) under Contract No. DE-AC52-07NA27344. It was supported by LLNL Laboratory Directed Research and Development Program Grant No. 15-ERD-065, by the DOE Office of Science, Fusion Energy Science under FWP100182, FWP100237 and by the DOE Early Career Research Program under FWP100331. Experimental time was provided through the DOE LBS program. Computing resources for this work came from the LLNL Institutional Computing Grand Challenge.

*Corresponding author.
swadling1@llnl.gov

[1] A. R. Bell, P. Choi, A. E. Dangor, O. Willi, D. A. Bassett, and C. J. Hooker, Collisionless shock in a laser-produced ablating plasma, Phys. Rev. A **38**, 1363 (1988).
[2] R. L. Berger, J. R. Albritton, C. J. Randall, E. A. Williams, W. L. Kruer, A. B. Langdon, and C. J. Hanna, Stopping and thermalization of interpenetrating plasma streams, Phys. Fluids B **3**, 3 (1991).
[3] T. N. Kato and H. Takabe, Nonrelativistic collisionless shocks in unmagnetized electron-ion plasmas, Astrophys. J. **681**, L93 (2008).
[4] H. Takabe *et al.*, High-Mach number collisionless shock and photo-ionized non-LTE plasma for laboratory astrophysics with intense lasers, Plasma Phys. Controlled Fusion **50**, 124057 (2008).
[5] C. Constantin *et al.*, Collisionless interaction of an energetic laser produced plasma with a large magnetoplasma, Astrophys. Space Sci. **322**, 155 (2009).
[6] Y. Kuramitsu *et al.*, Time Evolution of Collisionless Shock in Counterstreaming Laser-Produced Plasmas, Phys. Rev. Lett. **106**, 175002 (2011).
[7] J. S. Ross *et al.*, Characterizing counter-streaming interpenetrating plasmas relevant to astrophysical collisionless shocks, Phys. Plasmas **19**, 056501 (2012).
[8] D. D. Ryutov, N. L. Kugland, H. S. Park, C. Plechaty, B. A. Remington, and J. S. Ross, Basic scalings for collisionless-shock experiments in a plasma without pre-imposed magnetic field, Plasma Phys. Controlled Fusion **54**, 105021 (2012).
[9] N. L. Kugland *et al.*, Self-organized electromagnetic field structures in laser-produced counter-streaming plasmas, Nat. Phys. **8**, 809 (2012).
[10] W. Fox, G. Fiksel, A. Bhattacharjee, P.-Y. Chang, K. Germaschewski, S. X. Hu, and P. M. Nilson, Filamentation Instability of Counterstreaming Laser-Driven Plasmas, Phys. Rev. Lett. **111**, 225002 (2013).
[11] D. D. Ryutov, N. L. Kugland, M. C. Levy, C. Plechaty, J. S. Ross, and H. S. Park, Magnetic field advection in two interpenetrating plasma streams, Phys. Plasmas **20**, 032703 (2013).
[12] J. S. Ross, H.-S. Park, R. Berger, L. Divol, N. L. Kugland, W. Rozmus, D. Ryutov, and S. H. Glenzer, Collisionless Coupling of Ion and Electron Temperatures in Counterstreaming Plasma Flows, Phys. Rev. Lett. **110**, 145005 (2013).
[13] E. C. Merritt, A. L. Moser, S. C. Hsu, J. Loverich, and M. Gilmore, Experimental Characterization of the Stagnation Layer between Two Obliquely Merging Supersonic Plasma Jets, Phys. Rev. Lett. **111**, 085003 (2013).
[14] G. F. Swadling *et al.*, Shock-less interactions of ablation streams in tungsten wire array z-pinches, Phys. Plasmas **20**, 062706 (2013).

[15] G. F. Swadling *et al.*, Interpenetration, Deflection, and Stagnation of Cylindrically Convergent Magnetized Supersonic Tungsten Plasma Flows, Phys. Rev. Lett. **113**, 035003 (2014).
[16] G. F. Swadling *et al.*, Experimental investigations of ablation stream interaction dynamics in tungsten wire arrays: Interpenetration, magnetic field advection, and ion deflection, Phys. Plasmas **23**, 056309 (2016).
[17] C. M. Huntington *et al.*, Observation of magnetic field generation via the Weibel instability in interpenetrating plasma flows, Nat. Phys. **11**, 173 (2015).
[18] H.-S. Park *et al.*, Collisionless shock experiments with lasers and observation of Weibel instabilitiesa), Phys. Plasmas **22**, 056311 (2015).
[19] W. Fox, J. Park, W. Deng, G. Fiksel, A. Spitkovsky, and A. Bhattacharjee, Astrophysical particle acceleration mechanisms in colliding magnetized laser-produced plasmas, Phys. Plasmas **24**, 092901 (2017).
[20] P. Tzeferacos *et al.*, Laboratory evidence of dynamo amplification of magnetic fields in a turbulent plasma, Nat. Commun. **9**, 591 (2018).
[21] J. D. D. Hare *et al.*, Anomalous Heating and Plasmoid Formation in a Driven Magnetic Reconnection Experiment, Phys. Rev. Lett. **118**, 085001 (2017).
[22] C. M. M. Huntington *et al.*, Magnetic field production via the Weibel instability in interpenetrating plasma flows, Phys. Plasmas **24**, 041410 (2017).
[23] D. P. Higginson *et al.*, Kinetic effects on neutron generation in moderately collisional interpenetrating plasma flows, Phys. Plasmas **26**, 012113 (2019).
[24] J. S. Ross *et al.*, Transition from Collisional to Collisionless Regimes in Interpenetrating Plasma Flows on the National Ignition Facility, Phys. Rev. Lett. **118**, 185003 (2017).
[25] M. V. Medvedev and A. Loeb, Generation of magnetic fields in the relativistic shock of gamma-ray burst sources, Astrophys. J. **526**, 697 (1999).
[26] A. Gruzinov and E. Waxman, Gamma-ray burst afterglow: Polarization and analytic light curves, Astrophys. J. **511**, 852 (1999).
[27] A. Spitkovsky, Particle acceleration in relativistic collisionless shocks: Fermi process at last? Astrophys. J. **682**, L5 (2008).
[28] E. Weibel, Spontaneously Growing Transverse Waves in a Plasma due to an Anisotropic Velocity Distribution, Phys. Rev. Lett. **2**, 83 (1959).
[29] B. D. Fried, Mechanism for instability of transverse plasma waves, Phys. Fluids **2**, 337 (1959).
[30] R. C. Davidson, D. A. Hammer, I. Haber, and C. E. Wagner, Nonlinear development of electromagnetic instabilities in anisotropic plasmas, Phys. Fluids **15**, 317 (1972).
[31] J. Katz, R. Boni, C. Sorce, R. Follett, M. J. Shoup, and D. H. Froula, A reflective optical transport system for ultraviolet Thomson scattering from electron plasma waves on OMEGA, Rev. Sci. Instrum. **83**, 10E349 (2012).
[32] J. Sheffield, D. Froula, S. H. Glenzer, and N. C. Luhmann, Jr., *Plasma Scattering of Electromagnetic Radiation: Theory and Measurement Techniques*, 2nd ed. (Academic Press, Cambridge, 2010).
[33] See Supplemental Material at http://link.aps.org/supplemental/10.1103/PhysRevLett.124.215001 for examples of additional data.
[34] C. Ruyer, L. Gremillet, A. Debayle, and G. Bonnaud, Nonlinear dynamics of the ion Weibel-filamentation instability: An analytical model for the evolution of the plasma and spectral properties, Phys. Plasmas **22**, 032102 (2015).
[35] C. Ruyer and F. Fiuza, Disruption of Current Filaments and Isotropization of the Magnetic Field in Counterstreaming Plasmas, Phys. Rev. Lett. **120**, 245002 (2018).
[36] G. F. Swadling *et al.*, Calculation of Thomson scattering spectral fits for interpenetrating flows, AIP Conf. Proc. **1639**, 118 (2014).
[37] D. D. Ryutov, F. Fiuza, C. M. Huntington, J. S. Ross, and H.-S. Park, Collisional effects in the ion Weibel instability for two counter-propagating plasma streams, Phys. Plasmas **21**, 032701 (2014).
[38] R. A. Fonseca *et al.*, OSIRIS: A three-dimensional, fully relativistic particle in cell code for modeling plasma based accelerators, in *Comput. Sci.—ICCS 2002*, edited by P. M. A. Sloot and A. G. Hoekstra, C. J. K. Tan, and J. J. Dongarra (Springer Berlin Heidelberg, Berlin, Heidelberg, 2002), pp. 342–351.
[39] R. A. Fonseca, J. Vieira, F. Fiuza, A. Davidson, F. S. Tsung, W. B. Mori, and L. O. Silva, Exploiting multi-scale parallelism for large scale numerical modelling of laser wakefield accelerators, Plasma Phys. Controlled Fusion **55**, 124011 (2013).
[40] C. Bruulsema, On the local measurement of electric currents and magnetic fields using Thomson scattering in Weibel-unstable plasmas, Phys. Plasmas **27**, 052104 (2020).
[41] N. L. Kugland, D. D. Ryutov, C. Plechaty, J. S. Ross, and H.-S. Park, Invited article: Relation between electric and magnetic field structures and their proton-beam images, Rev. Sci. Instrum. **83**, 101301 (2012).
[42] H. Alfvén, On the motion of cosmic rays in interstellar space, Phys. Rev. **55**, 425 (1939).
[43] S. Göde *et al.*, Relativistic Electron Streaming Instabilities Modulate Proton Beams Accelerated in Laser-Plasma Interactions, Phys. Rev. Lett. **118**, 194801 (2017).
[44] A. Macchi, A. Antonicci, S. Atzeni, D. Batani, F. Califano, F. Cornolti, J. J. Honrubia, T. V. Lisseikina, F. Pegoraro, and M. Temporal, Fundamental issues in fast ignition physics: from relativistic electron generation to proton driven ignition, Nucl. Fusion **43**, 362 (2003).